UDK 67.017:620.1:544.526.5:546.766
Original scientific article/Izvirni znanstveni članek

ISSN 1580-2949
MTAEC9, 54(2)173(2020)

STUDY OF THE REDUCTION OF Cr(VI) USING A BIO-BASED g-C_3N_4/LSACF PHOTOCATALYST

ŠTUDIJA REDUKCIJE Cr(VI) Z UPORABO g-C_3N_4/LSACF BIOKATALIZATORJA

Binhua Luo, Hang Yang, Ermao Li, Boxun Zhou, Yue Wang, Pan Li, Shibin Xia*

College of Resource and Environment, Wuhan University of Technology, No. 171 Luoshi street, Hongshan District, 430000, Wuhan, China

Prejem rokopisa – received: 2019-07-25; sprejem za objavo – accepted for publication: 2019-11-29

doi:10.17222/mit. 2019.175

In this study a novel g-C_3N_4/LSACF composite photocatalyst was prepared and used for Cr(VI) reduction. The physical and chemical properties of the materials were measured by multiple characterization methods, including scanning electronic microscopy (SEM), X-ray diffraction (XRD), energy-dispersive X-ray (EDS), Fourier-transform infrared spectroscopy (FTIR), UV– Vis spectrophotometry and Brunauer Emmett Teller (BET). The effects of various factors, including kind of catalyst, dosage of catalyst, pH value, initial concentration of Cr(VI) and cycle number, on the Cr(VI) reduction were investigated. The results show the g-C_3N_4/LSACF composite photocatalyst exhibited better catalysis efficiency than a single g-C_3N_4 photocatalyst in Cr(VI) reduction. The recycling use of the g-C_3N_4/LSACF composite photocatalyst is available with a certain reduction efficiency after the fourth recycle. The presence of oxalic acid enhanced the photocatalytic reduction efficiency of Cr(VI). The obtained g-C_3N_4/LSACF composite photocatalyst has a promising application flexibility in pollutant treatment.

Keywords: reduction of Cr(VI), g-C3N4, LSACF, photocatalysis

V članku avtorji opisujejo študijo priprave in uporabe novega g-C_3N_4/LSACF kompozitnega fotokatalizatorja za redukcijo ionov šestvalentnega kroma (Cr(VI)). Fizikalne in kemijske lastnosti materialov so določali z več metodami in sicer: z vrstičnim elektronskim mikroskopom (SEM), z rentgensko difrakcijo (XRD), z energijsko disperzijo rentgenskih žarkov (EDS), z Fourierjevo transformacijsko infrardečo spektroskopijo (FTIR), z UV-Vis spektro-fotometrijo in z metodo določevanja specifične površine delcev po Brunauer-Emmett in Teller-ju (BET). Avtorji so raziskovali vpliv različnih faktorjev na redukcijo Cr(VI), vključno z vrsto in velikostjo doze katalizatorja, pH vrednosti, začetne koncentracije Cr(VI) in cikličnega števila. Rezultati analiz so pokazali, da je za redukcijo Cr(VI) bolj učinkovit g-C_3N_4/LSACF kompozitni katalizator kot samostojni g-C_3N_4 fotokatalizator. Po štirih ciklih recikliranja kompozitnega katalizatorja g-C_3N_4/LSACF, ga je z določeno stopnjo učinkovitosti možno spet uporabiti za redukcijo. Prisotnost oksalne kisline pospeši učinkovitost fotokatalitične redukcije Cr(VI). Izdelani g-C_3N_4/LSACF kompozitni fotokatalizator obeta njegovo fleksibilno uporabo pri uporabi obdelave vodnih onesnaževalcev.

Ključne besede: redukcija Cr(VI), g-C3N4, LSACF, fotokataliza

1 INTRODUCTION

Nowadays, the heavy-metal pollution problem in water is increasingly serious. Cr(VI) is a relatively common heavy-metal ion pollutant which is derived from the discharge of production wastewater in industrial production, such as metallurgy, the chemical industry, electroplating, leather making, industrial paint coating manufacturing.[1–4]

Compared with Cr(III), Cr(VI) has a higher toxicity and a stronger fluidity, which is about 100 times that of Cr(III).[5] A lot of studies have indicated the possible damages of Cr(VI), including cancer after inhalation, allergies after contact with human skin, and genetic diseases such as genetic mutation.[6–8] Environmentally dangerous hazards are also observed.[9] Therefore, it is urgent to take relevant treatment measures to treat Cr(VI)-containing wastewater or reduce it to Cr(III) with less toxicity.

Considerable measures were carried out for the heavy-metal wastewater treatment, such as adsorption,[10,11] advanced oxidation[12,13] and biological treatment.[14] However, traditional treatment was accompanied with some shortcomings, e.g., the strong toxicity of heavy metals to microorganisms.[15] Nowadays, visible-light catalysis technology has shown a very promising performance for reducing Cr(VI) due to its advantages of high efficiency, low energy consumption and no secondary pollution.

Graphitic-carbon nitride (g-C_3N_4), a promising catalyst, has been employed in the removal of many organic pollutants.[16] Generally, g-C_3N_4 is synthesized via a series of simple polycondensation reactions using precursors such as dicyandiamide and urea with no metal material.[17,18] The photocatalytic performance of g-C_3N_4 under visible light was extensively studied due its unique structure, electronic properties and low cost.[19,20] However, g-C_3N_4 has the defect of low utilization efficiency and difficulty in recycling.[21] To improve the utilization efficiency of the g-C_3N_4 in practice, supported g-C_3N_4 on LSACF was prepared in this work.

*Corresponding author's e-mail:
xiashibin@126.com (Shibin Xia)

Activated carbon fibre (ACF), a general carbon material, has been widely used in the adsorption, electrode materials and catalyst carriers due to the characteristics of large specific surface area and rich micropores.[22,23] In this paper, a luffa sponge with the tubular fibre frame of luffa was used as precursor to prepare bio-based ACF. On this basis, the g-C3N4/LSACF composite was prepared to avoid the defect in low utilization efficiency and difficulty in recycling in g-C3N4 catalyst

In this study Cr(VI) was selected as the target pollutant. The effect of g-C3N4/LSACF composite on its reduction under visible light was investigated. The effects of the dosage of composites, the initial concentration of the Cr(VI), the initial pH and the amount of oxalic acid (OA) were surveyed. The recycling properties of the composites were tested and the photocatalytic reduction was carried out. The mechanism of Cr(VI) reduction was analysed and speculated.

2 EXPERIMENTAL PART

2.1. Materials and instruments

Luffa sponge was purchased from Luohe Huahui Daily Necessities Co., Ltd. All the reagents employed include: urea, sodium chloride, hydrochloric acid, OA, sodium hydroxide, phenolic resin, potassium dichromate and diphenyl semicarbazide. All the agents were at analytical grade and applied without any further purification. An aqueous Cr(VI) solution was prepared using distilled water.

The spectrophotometric measurements of the Cr(VI) concentration were performed using UV–Vis spectrometer (UNICOWFUV-2). The BET analysis was performed by automatic surface area and a porosity analyser (ASAP 2020M). The EDS mapping analysis was employed using electric refrigeration spectrometer (X-Max50). The XRD analysis was performed on X-ray diffractometer (D8 Advance). The SEM analysis were carried out using a field-emission scanning electron microscope (JSM-IT300). The FTIR and UV-Vis analyses were made using a Fourier-transform infrared spectrometer (Nexus) and UV/Vis/NIR spectrophotometer (Lambda 750 S). All the general instruments employed include an electronic balance (BS223S), a tubular resistance furnace (SK2-4-12A), a box-type energy-saving resistance furnace (SK2-8-13), a centrifuge (TG16-II), a drying box (DGG-9123A), a magnetic stirrer (TWCL-D), a thermostatic oscillator (SHZ-82A), a photocatalytic light source (500W long arc xenon lamp).

2.2. Preparations of LSACF and g-C_3N_4/LSACF

Preparation of LSACF: Luffa sponge was soaked in a 2 % NaOH solution for 24 h, rinsed to neutral with deionized water, and dried in an oven at 105 °C. The resulted sample was immersed in phenolic resin solution with 37 % solids for 24 h, taken out in a cool place, and dried in an oven at 105 °C for 1.5 h. Then, the sample was pre-oxidized, carbonized and activated by a high-temperature tubular resistance furnace. The heating process of the resistance furnace is: heating at 8 °C/min to 200 °C, maintaining for 120 min, then heating to 750 °C, maintaining for 70 min, and then allowing it to cool naturally. The resistance furnace is fed with N_2 (flow rate is 0.7 L/min) as a protective gas. Finally, the product was immersed in a hydrochloric acid solution with a concentration of 1 mol/L for 2 h, then washed with deionized water until neutral, and dried, and the obtained product was luffa sponge activated carbon fibre (LSACF).

2.3. Preparation of g-C_3N_4/LSACF

The resulted LSACF was cut into small pieces with a certain volume, immersed in a urea supersaturated solution for ultrasonic vibration for 30 min, and then dried in an oven at 60 °C. Then it was placed in a crucible and wrapped with urea powder, placed in a high-temperature tubular resistance furnace with the temperature heated to 550 °C at a rate of 1–2 °C/min. The temperature is maintained for 3 h, and N_2 is used as a shielding gas with a flow rate of 0.7 L/min through the whole reaction. After naturally cooling to room temperature, the sample was taken out, flushed using a mixed solution of distilled water and ethanol with a volume ratio 1:1 until no powder on the surface, and dried at 60 °C. The resulting g-C_3N_4 / LSACF composite was obtained. After multiple weighing, the mass ratio of g-C_3N_4 to LSACF is around 1:15.

2.4. Batch experiments

LSACF, g-C_3N_4 powder and g-C_3N_4/LSACF composite materials were used as photocatalytic materials, and the Cr(VI) solution with a certain volume (200 mL) and concentration was used as the target pollutant. Dilute sulfuric acid (0.1 mol/L) and NaOH (0.1 mol) were used to adjust the pH of the solution. At the beginning of the test, the light source was turned off for 60 min in the dark environment for the adsorption-desorption equilibrium, and the photocatalytic test was carried out as the zero time point. The solution was sampled at regular intervals for determining the concentration of Cr. The recyclability is a critical property for photocatalytic materials. In this study, the recyclability test was performed for the reduction of Cr(VI) four times. After each use, the mixed solution was taken out, rinsed thoroughly using distilled water and alcohol (volume ratio of 1:1), and dried at 60 °C. In addition, OA was selected as a sacrificial agent in order to explore the role of the sacrificial agent.[24] The experimental conditions are presented in detail in **Table 1**.

Table 1: Experimental conditions

Set	Object	Type of catalyst	Additional OA (g/L)	pH	Dosage of catalyst (g/L)	Initial Gr(VI) concentration (mg/L)	Reaction time (min)
1	Effect of four conditions	LSACF, g-C_3N_4 g-C_3N_4 /LSACF , and g-C_3N_4 /LSACF+OA	0/0.2	3	12	10	0-240
2	Effect of catalyst dosage	g-C_3N_4 /LSACF	0.2	3	12/14/18/ 21/24	10	60+ 0-180
3	Effect of initial Gr(VI) concentration	g-C_3N_4 /LSACF	0.2	3	18	5/10/20/30	60+ 0-180
4	Effect of pH	g-C_3N_4 /LSACF	0.2	3/5 7/9	18	10	60+ 0-180
5	Effect of cycle number	g-C_3N_4 /LSACF	0.2	5	18	10	0-240
6	Effect of OA	g-C_3N_4 /LSACF	0/0.2/0.4/ 0.6/0.8	5	18	10	240

2.5. Determination of Cr

The concentration of Cr(VI) was tested using diphenylcarbazide spectrophotometry. The reduction rate of the Cr(VI) (%) was calculated using Equation (1):

$$\text{Reduction rate} = \left(1-\frac{c}{c_0}\right)\cdot 100\ \% \quad (1)$$

where c_o is the initial concentration of Cr(VI) in the solution (mg/L); c is the concentration of Cr(VI) in the solution at a fixed time (mg/L).

3 RESULTS AND DISCUSSION

3.1. Characterization of the materials

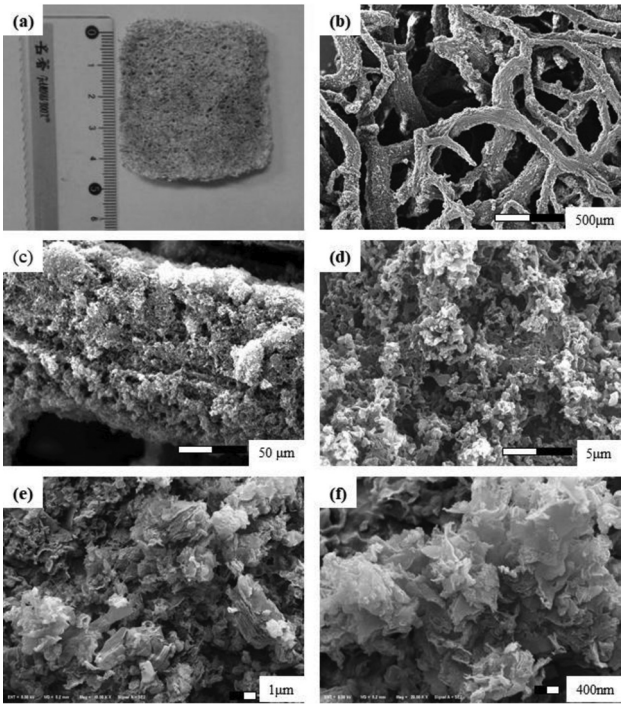

Figure 1: a) Photographs of sample, (b, c, d) SEM images of g-C_3N_4/LSACF and (e, f) g-C_3N_4

The morphologies of the samples are shown in **Figure 1a** the LSACF surface is covered with a light-yellow powder. **Figures 3** (**b-d**) show the SEM images of g-C_3N_4/LSACF at different magnifications. In **Figure 1b** the fibres are wrapped by g-C_3N_4 powder on the surface. **Figure 1c** shows that g-C_3N_4 is tightly covered on the

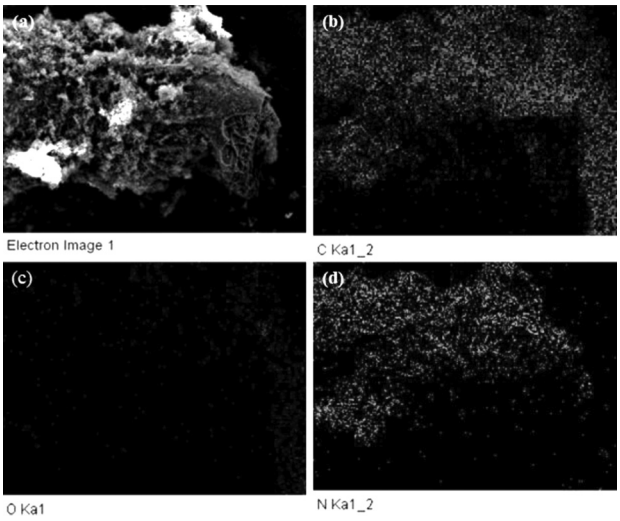

Figure 2: a) SEM and b), c), d) elemental mapping images of simple fibre

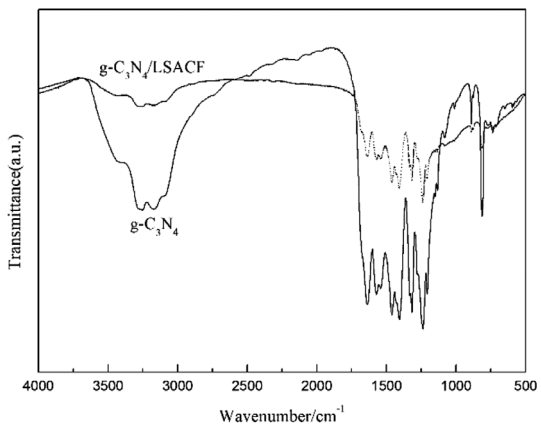

Figure 3: FTIR-spectra of g-C_3N_4 and g-C_3N_4/LSACF

single fibre. Under a larger magnification, the layered porous structure of g-C_3N_4 can be seen through **Figure 1d** due to the gas derived from the decomposition of urea promoting the formation of the porous structure of g-C_3N_4 during the condensation process; it can be seen from **Figures 1e** and **1f** that g-C_3N_4 has a distinct lamellar structure, which was confirmed in the subsequent XRD test results.

Table 2: Surface area, pore volume and average pore radius of samples

Sample	Specific area /(m^2/g)	Volume /(cm^3/g)	$R_{average}$/nm
g-C_3N_4	68.01	0.4191	24.65
g-C_3N_4/LSACF	105.4	0.1676	6.360

The EDS mapping analysis was employed to determine the distribution of elements on a single fibre. As can be seen from **Figure 2**, in addition to the C element, N and O elements also appear. The C and N elements are distributed substantially uniformly on the fibre surface. The O element present due the raw material for LSACF and phenolic resin employed during preparation, which contains a large amount of O element.

Figure 3 shows the FTIR spectrum of pure g-C_3N_4 powder and g-C_3N_4/LSACF composite. The absorption peak of g-C_3N_4 powder at 808 $cm^{-1}$is the characteristic absorption peak of the triazine ring structure. The continuous strong absorption peak at 1200-1670 cm^{-1} is ascribed to the stretching and vibration of the CN bond. The wide absorption peak at 3000–3400 cm^{-1} corresponds to the vibration of the NH bond. Compared with the spectrum of the g-C_3N_4/LSACF composite, the main absorption peak of the above g-C_3N_4 appears in the composite material, and there is no large shift in the absorption peak position, indicating that g-C_3N_4 has been successfully loaded on the carbon fibre, and the properties have not changed greatly.

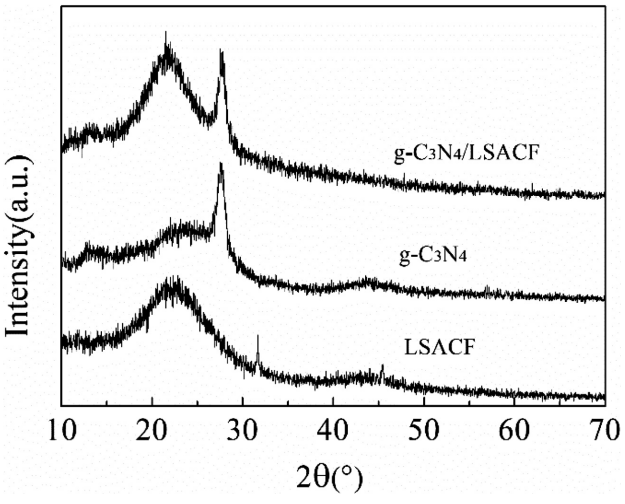

Figure 4: XRD patterns of LSACF, g-C_3N_4 and g-C_3N_4/LSACF

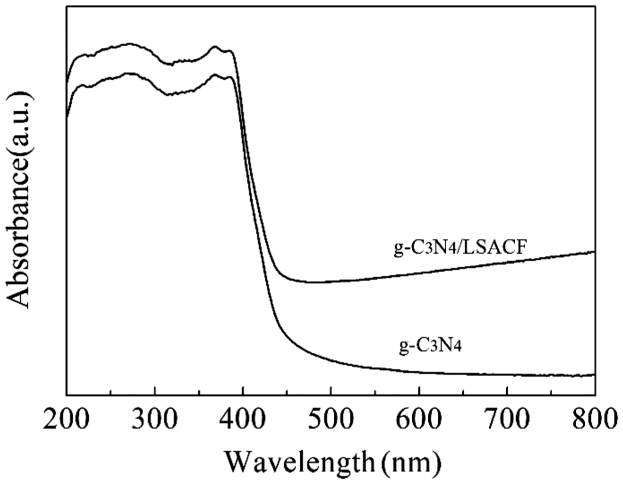

Figure 5: UV-vis diffuse reflection spectra of g-C_3N_4 and g-C_3N_4/LSACF

Figure 4 shows the XRD spectra of the g-C_3N_4/LSACF composite, LSACF and g-C_3N_4 powder, respectively. It can be seen from the figure that LSACF has a broad diffraction peak only around 22°, while g-C_3N_4 powder has obvious diffraction peaks around 13.2° and 27.4°, corresponding to the diffraction plane of the graphite carbonitride material (100) and (002), respectively. The peak at 27.4° belongs to the interlaminar accumulation of the conjugated aromatic system, indicating a certain lamellar structure. The g-C_3N_4/LSACF composite has a peak of LSACF around 22° and characteristic peaks of g-C_3N_4 at 13.2° and 27.4°, indicating that g-C_3N_4 is loaded on the LSACF fibre.

Figure 5 shows the UV-visible diffuse reflectance spectra of pure g-C_3N_4 powder and g-C_3N_4/LSACF composites. The absorption band edge of pure g-C_3N_4 powder is about 450 nm, similar to previous reports.[25] Compared with the pure g-C_3N_4 absorption band, the composite material has a slight red shift at 455 nm and

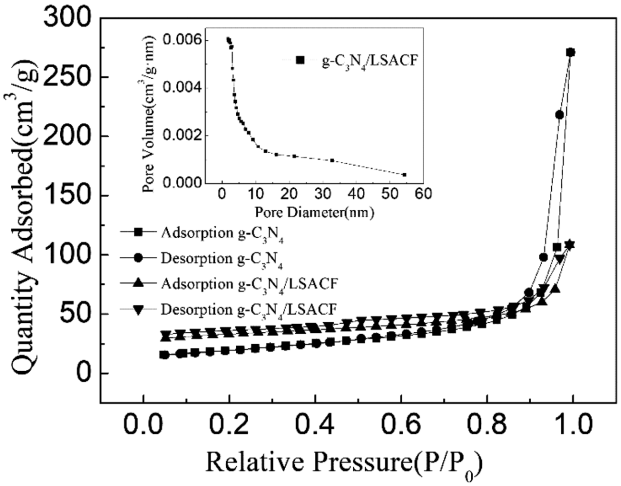

Figure 6: N_2 adsorption-desorption isotherms of g-C_3N_4, g-C_3N_4/LSACF and pore size distribution of g-C_3N_4/LSACF

the calculated forbidden band of g-C_3N_4/LSACF is about 2.73 eV. The absorption value in the long wavelength band is up due to the porous structure of LSACF and scattered light in the fibre.

Figure 6 shows the N_2 adsorption-desorption curve of pure g-C_3N_4 powder and g-C_3N_4/LSACF composites, both of which are roughly expressed as type-IV isotherms. Compared to pure g-C_3N_4 the shape of g-C_3N_4/LSACF does not change obviously. A hysteresis loop occurs in the higher-pressure ratio (0.9-1.0), which may be the capillary condensation caused by the sample mesopores. According to the classification of the hysteresis loop in the IUPAC, the hysteresis loop in **Figure 6** belongs to the H_2 type, indicating the porous structure, which is consistent with the results of the SEM image analysis. From the pore size distribution map, the composite material contains more mesopores. It can be seen from **Table 2** that the specific surface area of the composite material increases after loading. However, the pore volume and average pore size are reduced in g-C_3N_4/LSACF, which may be caused by a slight agglomeration of g-C_3N_4 on the fibre surface.

3.2. Batch experiments

Figure 7a indicates the effect of four conditions on Cr(VI) removal. It can be seen from **Figure 7a** that after 140 min of reduction, the removal rates of Cr(VI) were 9.0 %, 35.9 %, 53.3 % and 81.2 % using LSACF, g-C_3N_4, LSACF/g-C_3N_4 and LSACF/g-C_3N_4 +OA, respectively. Compared with the final removal effects of the others, LSACF/g-C_3N_4 +OA showed the best reduction efficacy. In addition, the removal rate of Cr(VI) by g-C3N4/LSACF was significantly higher than that of g-C3N4 or LSACF, and the addition of OA as a sacrificial agent significantly improved the catalytic activity.

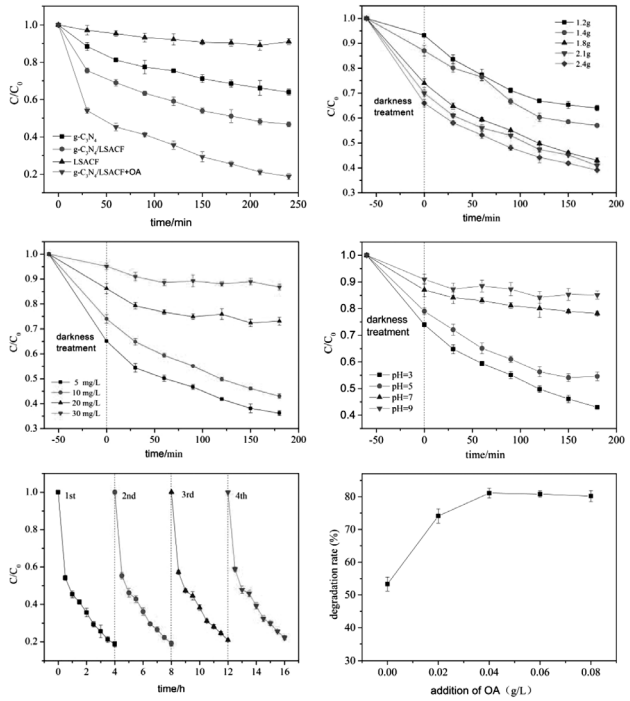

Figure 7: Batch experiments: a) the effect of four conditions, b) effect of catalyst dosage, c) effect of initial Cr(VI) concentration, d) effect of pH, e) effect of cycle number, f) additional OA

Figure 7b indicates the effect of catalyst dosage on Cr(VI) removal. It can be seen from the figure that in the dark treatment, the adsorption removal rate of Cr(VI) is gradually increased with the increasing dosage of catalyst. After the dark treatment, the final removal rate of Cr(VI) also increases gradually with an increase of the catalyst dosage, and reaches the maximum value, 60.9%, when the dosage is 24 g/L. However, the removal rate of 60.9% was obtained with the dosage of 18 g/L. The possible reason is due to that the effective catalytic area saturation was reached when the catalyst dosage is 18 g/L, and the excessive catalyst dosage does not lead to an increase in the effective number of active sites, and the photocatalytic reduction efficiency. Therefore, the optimum dosage was set at 18 g/L.

Figure 7c indicates the effect of initial Cr(VI) concentration on Cr(VI) removal. It can be seen from the figure that the catalyst has certain reduction and removal effects on different concentrations of Cr(VI), but the reduction efficiency is significantly higher at a low concentration than that under high concentration conditions, which resulted from the lower propagation of light in the solution with higher Cr(VI) concentration. On the other hand, the adsorption of more solute on the catalyst leads to a decrease in the surface catalytic activity sites. Therefore, the composite material is suitable for the catalytic reduction of lower concentrations of Cr(VI).

Figure 7d indicates the effect of pH on Cr(VI) removal. It can be seen from the figure that the amount of Cr(VI) adsorbed by the composite decreases with increasing pH value. After the light is turned on, the photocatalytic reduction efficiency of the composite under acidic conditions was significantly higher than that for neutral or alkaline conditions. In addition, the better reduction effect was obtained with greater acidity. This is because, under acidic conditions, the presence of Cr(VI) in solution is mainly $HCrO^{-4}$, while the surface of g-C_3N_4 is positively charged, and the positive and negative phase absorption causes the Cr(VI) to be rapidly reduced to trivalent, as in Equation 2. At the same time, the trivalent chromium that is reduced under neutral or alkaline conditions will form a $Cr(OH)_3$ precipitate covering the surface of the catalyst, resulting in a decrease in the effective active sites of the catalyst.[26,27] On the other hand, the Nernst equation (Equation 3) we can see that when the H^+ concentration in the acidic solution is larger, the corresponding electrode potential is larger, and the Cr(VI) is more likely to be reduced.[13,28] Therefore, the photocatalytic reduction of Cr(VI) is more advantageous in acidic conditions.

$$HCrO\text{-}4 + 7H^+ + 3e^- \rightarrow Cr^{3+} + 4H_2O \quad (2)$$

$$\varphi = \varphi^{\theta} + \frac{RT}{6F} \ln \frac{[Cr_2O_7^{2-}] \cdot [H^+]}{[Cr^{3+}]} \quad (3)$$

Figure 7e shows the cycle number of Cr(VI) reduction by g-C_3N_4/LSAC. The results showed that the reduction rate of 80% could be obtained after four uses, which shows a good recycling performance of g-C_3N_4/LSACF.

Figure 7f shows the effect of OA concentration on the reduction of Cr(VI) by g-C_3N_4/LSACF. As shown in the figure, the addition of the sacrificial OA greatly improved the reduction removal rate of Cr(VI). The reduction efficiency of Cr(VI) increased with the low concentration of the sacrificial agent, and decreased slightly after 0.04 g/L. The reason for this is that at low concentrations, OA acts as an electron donor, and its concentration increases with the g-C_3N_4/LSACF photogenerated holes, thereby promoting more photogenerated electron release to reduce Cr(VI). However, the high concentration of OA competes with Cr(VI) for adsorption and even adheres to the surface of the catalyst, resulting in a slight decrease in the catalytic efficiency.

According to the experimental analysis, the reaction mechanism for the reduction of Cr(VI) was investigated. As shown in Figure 8, electron-hole pairs are generated under the irradiation of visible light, and involved in the oxidation reaction of the pollutants. The photogenerated electrons are trapped by the O_2 in the solution to form superoxide radicals to reduce Cr(VI). In addition, OA acts as an electron donor, which can react with the generated holes in time and the timely consumption of holes improves the separation efficiency of the photogenerated electrons and holes. Besides, the total chromium concentration was measured to speculate about the possible changing forms of Cr(VI) in the process of photocatalytic degradation. The total chromium concentration remains constant after catalysis reaction, indicating that all the Cr(VI) is reduced to Cr(III). Y. Zhao et Al.[29] have studied the photo-reduction of Cr(VI) using reduced graphene oxide decorated with TiO_2 nanoparticles, the reduction rate of Cr(VI) is up to 86.5 % and Cr(VI) is reduced to Cr(III). However, the expenditure for reduced graphene oxide is more expensive, while the g-C_3N_4/LSACF composite catalyst is more economic and available.

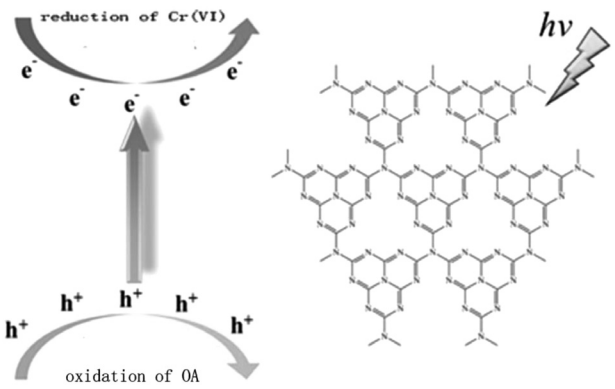

Figure 8: Mechanism of Cr(VI) reduction by g-C_3N_4/LSACF under visible light

4 CONCLUSIONS

A g-C_3N_4/LSACF composite photocatalyst was prepared using the impregnation method. Many characterization methods were employed to characterize the properties of g-C_3N_4/LSACF. The results of the characterization show g-C_3N_4 powder was even covered on the surface of the LSACF. Compared to other conditions, g-C_3N_4/LSACF+OA gave the optimal performance for the Cr(VI) reduction.

The dosage of the catalyst, the initial concentration of Cr(VI) and the pH value play an important role in the removal rate of Cr(VI). In addition, the results show that the removal of Cr(VI) was attributed to both the adsorption and catalytic effects of g-C_3N_4/LSACF. The result of four cycles shows the good recycling capability of g-C_3N_4/LSACF. The addition of the sacrificial OA greatly improves the efficiency of the photocatalytic reduction of Cr(VI).

Acknowledgment

The authors sincerely thank the funds for Study on Comprehensive Control of Rocky Desertification and Ecological Service Function Improvement in Karst Peaks (No. 2016YFC0502402).

5 REFERENCES

[1] K. Gong, H. Qian, Y. Lu, L. Min, D. Sun, S. Qian, B. Qiu, Z. Guo, Ultrasonic Pretreated Sludge Derived Stable Magnetic Active Carbon for Cr(VI) Removal from Wastewater, Acs Sustainable Chemistry & Engineering, 6 (**2018**) 7283–7291, 10.1021/acssuschemeng.7b04421

[2] D. M. Chen, C. X. Sun, C. S. Liu, M. Du, Stable Layered Semiconductive Cu(I)-Organic Framework for Efficient Visible-Light-Driven Cr(VI) Reduction and H2 Evolution, Inorganic Chemistry, 57 (**2018**) 7975–7981, 10.1021/acs.inorgchem.8b01137

[3] H. Lu, J. Wang, L. Fei, H. Xin, B. Tian, H. Hao, Highly Efficient and Reusable Montmorillonite/Fe3O4/Humic Acid Nanocomposites for Simultaneous Removal of Cr(VI) and Aniline, Nanomaterials, 8 (**2018**) 537–545, 10.3390/nano8070537

[4] P. Kar, T. K. Maji, P. K. Sarkar, P. Lemmens, S. K. Pal, Development of a Photo-Catalytic Converter for Potential Use in the Detoxification of Cr(VI) Metal in Water from Natural Resources, Journal of Materials Chemistry A, 6 (**2018**) 211–232, 10.1039/C7TA11138J

[5] P. Khare, A. Bhati, S. R. Anand, Gunture, S.K. Sonkar, Brightly Fluorescent Zinc-Doped Red-Emitting Carbon Dots for the Sunlight-Induced Photoreduction of Cr(VI) to Cr(III), ACS Omega, 3 (**2018**) 5187–5194, 10.1021/acsomega.8b01011

[6] G. Hu, P. Li, X. Cui, Y. Li, J. Zhang, X. Zhai, S. Yu, S. Tang, Z. Zhao, J. Wang, Cr(VI)-induced methylation and down-regulation of DNA repair genes and its association with markers of genetic damage in workers and 16HBE cells, Environmental Pollution, 238 (**2018**) 833–843, 10.1016/j.envpol.2018.03.046

[7] N. Husain, R. Mahmood, 3,4-Dihydroxybenzaldehyde quenches ROS and RNS and protects human blood cells from Cr(VI)-induced cytotoxicity and genotoxicity, Toxicology in Vitro An International

Journal Published in Association with Bibra, 50 (**2018**) 293–305, 10.1016 /j.tiv.2018.04.004

[8] Y. Xiao, M. Zeng, L. Yin, N. Li, F. Xiao, Clusterin increases mitochondrial respiratory chain complex I activity and protects against hexavalent chromium-induced cytotoxicity in L-02 hepatocytes, Toxicology Research, 8 (**2019**) 325–341 10.1039/C8TX00231B

[9] Y. He, H. Sun, W. Liu, W. Yang, A. Lin, Study on removal effect of Cr(VI) and surface reaction mechanisms by bimetallic system in aqueous solution, Environmental Technology, (**2018**) 1–23, 10.1080/09593330.2018.1551431

[10] A. K. Sharma, R. S. Devan, M. Arora, R. Kumar, Y. R. Ma, J. N. Babu, Reductive-co-precipitated cellulose immobilized zerovalent iron nanoparticles in ionic liquid/water for Cr(VI) adsorption, Cellulose, 25 (**2018**) 5259–5275, 10.1007/s10570-018-1932-y

[11] Y. Sun, C. Liu, Y. Zan, G. Miao, H. Wang, L. Kong, Hydrothermal Carbonization of Microalgae (Chlorococcum sp.) for Porous Carbons With High Cr(VI) Adsorption Performance, Applied Biochemistry & Biotechnology, (**2018**) 1–11, 10.1007/s12010-018-2752-0

[12] A. Thirumoorthi, D. S. Bhuvaneshwari, K. P. Elango, Preferential solvational effects on the Cr(VI) oxidation of benzylamines in benzene/2-methylpropan-2-ol mixtures, International Journal of Chemical Kinetics, 42 (**2010**) 159–167, 10.1002/kin.20464

[13] C. Fei, Y. Qi, Y. Wang, F. Yao, Y. Ma, X. Huang, X. Li, D. Wang, G. Zeng, H. Yu, Efficient construction of bismuth vanadate-based Z-scheme photocatalyst for simultaneous Cr(VI) reduction and ciprofloxacin oxidation under visible light: Kinetics, degradation pathways and mechanism, Chemical Engineering Journal, 348 (**2018**) 157–170, 10.1016/j.cej.2018.04.170

[14] N. M. Dogan, C. Kantar, S. Gulcan, C. J. Dodge, B. C. Yilmaz, M. A. Mazmanci, Chromium(VI) Bioremoval by Pseudomonas Bacteria: Role of Microbial Exudates for Natural Attenuation and Biotreatment of Cr(VI) Contamination, Environmental Science & Technology, 45 (**2011**) 2278–2285, 10.1021/es102095t

[15] C. Karthik, P. I. Arulselvi, Biotoxic Effect of Chromium (VI) on Plant Growth-Promoting Traits of Novel Cellulosimicrobium funkei Strain AR8 Isolated from Phaseolus vulgaris Rhizosphere, Geomicrobiology Journal, 34 (**2017**) 434–442, 10.1080/01490451.2016.1219429

[16] J. Chu, H. X, Y. Z, D. Y, S. B, X. P, Highly Efficient Visible-Light-Driven Photocatalytic Hydrogen Production on CdS/Cu7S4/g-C3N4 Ternary Heterostructures, Acs Applied Materials & Interfaces, 10 (**2018**) 20404–20411, 10.1021/acsami.8b02984

[17] L. Chao, H. Zhu, Y. Zhu, P. Dong, H. Hou, Q. Xu, X. Chen, X. Xi, W. Hou, Ordered layered N-doped KTiNbO5/g-C3N4 heterojunction with enhanced visible light photocatalytic activity, Applied Catalysis B Environmental, 228 (**2018**) 54–63, 10.1016/j.apcatb.2018.01.074

[18] S. Lamkhao, G. Rujijanagul, C. Randorn, Fabrication of g-C3N4 and a promising charcoal property towards enhanced chromium(VI) reduction and wastewater treatment under visible light, Chemosphere, 193 (**2018**) 237–243, 10.1016/j.chemosphere.2017.11.015

[19] A. Hatamie, F. Marahel, A. Sharifat, Green synthesis of graphitic carbon nitride nanosheet (g-C3N4) and using it as a label-free fluorosensor for detection of metronidazole via quenching of the fluorescence, Talanta, 176 (**2018**) 518–525, 10.1016/j.talanta.2017.08.059

[20] N. Misra, V. Kumar, S. Rawat, N.K. Goel, S.A. Shelkar, Jagannath, R.K. Singhal, L. Varshney, Mitigation of Cr(VI) toxicity using Pd-nanoparticles immobilized catalytic reactor (Pd-NICaR) fabricated via plasma and gamma radiation, Environmental Science & Pollution Research, (**2018**) 1–10, 10.1007/s11356-018-1709-8

[21] Y. J. Yuan, Y. Yan, Z. Li, D. Chen, S. Wu, G. Fang, W. Bai, M. Ding, L. X. Yang, D.-P. Cao, Promoting Charge Separation in g-C3N4/Graphene/MoS2 Photocatalysts by Two-Dimensional Nanojunction for Enhanced Photocatalytic H2 Production, ACS Applied Energy Materials, 1 (**2018**) 1400–1407, 10.1021/acsaem.8b00030

[22] S. Wang, X. Li, H. Zhao, X. Quan, S. Chen, H. Yu, Enhanced adsorption of ionizable antibiotics on activated carbon fiber under electrochemical assistance in continuous-flow modes, Water Research, 134 (**2018**) 162–169, 10.1016/j.watres.2018.01.068

[23] W. Ying, F. Yuan, W. Lu, L. Nan, W. Chen, Oxidative removal of sulfa antibiotics by introduction of activated carbon fiber to enhance the catalytic activity of iron phthalocyanine, Microporous & Mesoporous Materials, 261 (**2018**) 98–104, 10.1016/j.micromeso.2017.10.055

[24] Z. Xu, S. Bai, J. Liang, L. Zhou and Y. Photocatalytic reduction of Cr(VI) by citric and oxalic acids over biogenetic jarosite, Mater Sci Eng C Mater Biol Appl, Lan, 33 (**2013**) 2192–2196, 10.1016/j.msec.2013.01.040

[25] S. Sun, M. Sun, Y. Fang, W. Ying, H. Wang, One-step in situ calcination synthesis of g-C3N4/N-TiO2 hybrids with enhanced photoactivity, Rsc Advances, 6 (**2016**) 13063–13071, 10.1039/C5RA26700E

[26] L. D. Palma, N. Verdone, G. Vilardi, Kinetic Modeling of Cr(VI) Reduction by nZVI in Soil: The Influence of Organic Matter and Manganese Oxide, Bulletin of Environmental Contamination & Toxicology, (**2018**) 1–6, 10.1007/s00128-018-2394-5

[27] N. A. Oladoja, E. T. Anthony, I. A. Ololade, T. D. Saliu, G. A. Bello, Self-propagation combustion method for the synthesis of solar active Nano Ferrite for Cr(VI) reduction in aqua system, Journal of Photochemistry & Photobiology A Chemistry, 353 (**2018**) 229–239, 10.1016/j.jphotochem.2017.11.026

[28] Y. Zhang, J. Yang, L. Zhong, L. Liu, Effect of multi-wall carbon nanotubes on Cr(VI) reduction by citric acid: Implications for their use in soil remediation, Environmental Science & Pollution Research, 25 (**2018**) 1–8, 10.1007/s11356-018-2438-8

[29] Y. Zhao, D. Zhao, C. Chen, Enhanced photo-reduction and removal of Cr(VI) on reduced graphene oxide decorated with TiO2 nanoparticles, Journal of Colloid and Interface Science, 405 (**2013**) 211–217, 10.1016/j.jcis.2013.05.004